

# Medical imaging with mercuric iodide direct digital radiography flat-panel X-ray detectors

H. Gilboa, A. Zuck, O. Dagan, A. Vilensky, B.N. Breen, A. Taieb, B. Reisman and H. Hermon  
Real-Time Radiography, Jerusalem Technology Park, Jerusalem 91487 Israel.

G. Zentai, L. Partain

Ginzton Technology Center, Mountain View, CA 94043 USA

R. Street, S. Ready

Xerox Palo Alto Research Center, Palo Alto, CA94304 USA

## ABSTRACT

Photoconductive polycrystalline mercuric iodide coated on amorphous silicon flat panel thin film transistor (TFT) arrays is the best candidate for direct digital X-ray detectors for radiographic and fluoroscopic applications in medical imaging.

The mercuric iodide is vacuum deposited by Physical Vapor Deposition (PVD). This coating technology is capable of being scaled up to sizes required in common medical imaging applications. Coatings were deposited on 2"X2" and 4"X4" TFT arrays for imaging performance evaluation and also on conductive-coated glass substrates for measurements of X-ray sensitivity and dark current. TFT arrays used included pixel pitch dimensions of 100, 127 and 139 microns. Coating thickness between 150 microns and 250 microns were tested with beam energy between 25 kVP and 100 kVP utilizing exposure ranges typical for both fluoroscopic, and radiographic imaging.

X-ray sensitivities measured for the mercuric iodide samples and coated TFT detectors were superior to any published results for competitive materials (up to 7100 ke/mR/pixel for 100 micron pixels). It is believed that this higher sensitivity can result in fluoroscopic imaging signal levels high enough to overshadow electronic noise. Diagnostic quality of radiographic and fluroscopic images of up to 15 pulses per second were demonstrated. Image lag characteristics appear adequate for fluoroscopic rates. Resolution tests on resolution target phantoms showed that resolution is limited to the TFT array Nyquist frquency including detectors with pixel size of 139 microns resolution ~3.6 lp/mm) and 127 microns (resolution ~3.9 lp/mm). The ability to operate at low voltages (~0.5 volt/ micron) gives adequate dark currents for most applications and allows low voltage electronics designs.

**Keywords:** imaging, X-ray radiology, polycrystalline, mercuric iodide, imaging detectors, Flat-Panel imaging arrays.

## 1. INTRODUCTION

Direct detector materials need to have several attributes, including high x-ray absorption, high charge collection, low dark current, good uniformity etc., and these are difficult to achieve in a single material. Nevertheless, higher resolutions are possible with direct detectors than those attainable by detectors that utilize phosphor coatings.

|   | <b>Poly-HgI<sub>2</sub></b> | <b>a-Se</b>                         | <b>Comments</b>                                  |
|---|-----------------------------|-------------------------------------|--|
| Atomic Number (Z)   | 80, 53                      | 34                                  | Absorption increases with Z                      |
| Energy Band Gap (E <sub>g</sub> ) eV                        | 2.1                         | 2.2                                 | Wide gap reduces dark current                    |
| Charge Pair Formation Energy (W), eV                        | 5.5                         | 42                                  | Lower W increases the gain                       |
| Mobility Life-time Product ( $\mu\tau$ ) cm <sup>2</sup> /V | 1.5*10 <sup>-5</sup>        | 10 <sup>-6</sup> – 10 <sup>-5</sup> | Higher $\mu\tau$ increases the charge collection |
| Operational Electric Field (E) V/micron                     | 0.5-1                       | 10                                  | Lower E reduces electrical breakdown             |
| Processing Temperature (°C)                                 | 100                         | 400                                 | Lower temperature – simpler process              |

Table 1. Comparison of Amorphous Se and Poly HgI<sub>2</sub>

Polycrystalline semiconductor HgI<sub>2</sub> films directly convert X-rays into electrical signals and show promise as X-ray detectors for digital radiography<sup>1-13</sup>. Table 1 summarises film properties of amorphous Se and polycrystalline HgI<sub>2</sub> which are the materials considered for direct imaging. This paper describes measurements performed on high-resolution image sensors using HgI<sub>2</sub> photoconducting layers in the direct detection mode of operation.

The high Z value of HgI<sub>2</sub> indicates that it is an efficient material for absorbing X-rays for clinically used X-ray exposure energies. In addition, the X-ray energy required to generate an Electron-Hole Pair in the mercuric iodide photoconductor, as designated by the parameter W, is relatively low. The lower the W, the higher the number of charges caused by irradiation, and the higher the X-ray sensitivity. As Table 1 indicates, the parameter W is smaller for HgI<sub>2</sub> compared to Se by a factor of 7.

The larger the Mobility-Lifetime ( $\mu\tau$ -Product), the greater the distance the electrical charges move in the detector. Greater distances result in higher sensitivity due to better charge collection. The high Z number, low W and high  $\mu\tau$ -product result in very high signal which can overcome all noise sources in fluoroscopic modes of operation. The ability to operate at low voltages allows low voltage electronic design.

Mercuric iodide can be manufactured using very low temperature processing. This allows simple manufacturing techniques, a greater choice of substrate materials, and less danger of damaging the expensive TFTs during the coating process. This low manufacturing temperature will also allow the use of TFTs coated on plastic substrates, when they become available in the future. Plastic substrates offer cost-effective parts that lack brittleness and fragility, characteristically seen in the currently used glass. The temperature stability of HgI<sub>2</sub> allows operation, storage and transport at normally encountered temperatures. Other materials, such as amorphous selenium, have storage and transport problems that require them to be shipped and stored under special conditions. Even under non-extreme temperatures, amorphous selenium can irreversibly recrystallize, ceasing to act as a detector.

## 2. THEORETICAL RESULTS

### 2.1 Photon attenuation

Calculated graphs of photon attenuation efficiency (PAE) for polycrystalline Mercuric Iodide and amorphous Selenium are shown in Figure 1 for 70 kVp and 120 kVp with added 18 mm Al filtration. The graphs were obtained by using semi-empirical computer-generated spectra (TASMIP model)<sup>14</sup>, mass-attenuation coefficients taken from the NIST tables<sup>15</sup>, and the following equation for calculating the photon attenuation efficiency (PAE)<sup>16</sup>:

$$PAE = \frac{\int_{E=0}^{E=E_{max}} \Phi(E)(1 - e^{-\mu(E)\rho x})dE}{\int_{E=0}^{E=E_{max}} \Phi(E)dE} \quad (1)$$

where  $\Phi(E)$  is the spectral photon fluence,  $\mu(E)$  is the energy-dependent attenuation coefficient,  $\rho$  is the absorber coating density and  $x$  its thickness.

Since high attenuation is a necessary condition for high DQE (Detective Quantum Efficiency), one can conclude from Fig 1 that HgI<sub>2</sub> film thickness of 300 microns will result in >80% of photon attenuation at 70 kVp whereas for Se the film thickness is >1000 microns. For 120 kVp, film thickness of 500 micron of HgI<sub>2</sub> will attenuate the X-ray more than 80% whereas for Se, more than 2000 microns is needed to attenuate this amount of photons.

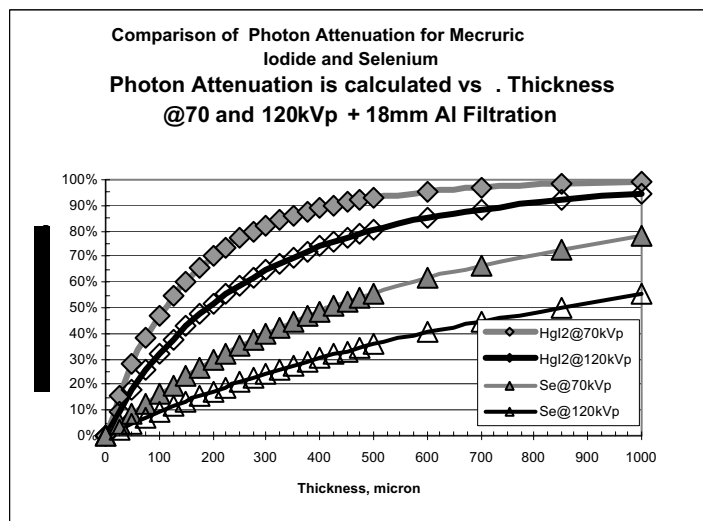


Fig. 1: Photon attenuation of HgI<sub>2</sub> and Se at 70kVp and 120 kVp with added filtration of 18 mm Al.

Photon attenuation is also dependent upon beam quality, as one can see from the theoretical modeling in Fig 2. This dependence needs to be considered in the image correction procedures performed by the readout electronics and software.

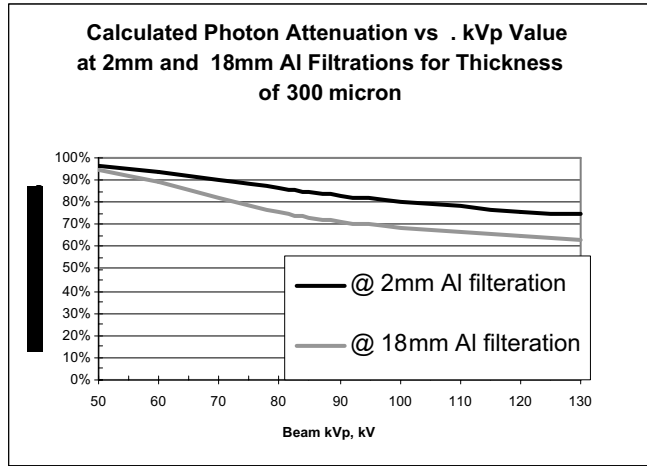


Fig2. Photon attenuation as a function of beam energy for added filtration of 2 mm and 18 mm Al. Film thickness is 300 microns

### 3. EXPERIMENTAL RESULTS

#### 3.1 X-ray transmission

X-ray transmission of glass substrates without an  $HgI_2$  layer were measured and these dose rate levels were taken into consideration for consequent measurements of X-ray transmission through different thickness of  $HgI_2$  layers that were deposited on the same type of glass substrates. Each tested value of transmission was averaged over three sequential measurements. The reading spread of the Radcal dosimeter ranged from 0.15% to 0.43%.

Fig 3 shows that a 300 micron film will absorb more than 80% of the X ray photons and that the absorption depends on the beam quality. These data can be compared to the theoretical calculation of transmission using NIST data for 50 keV.

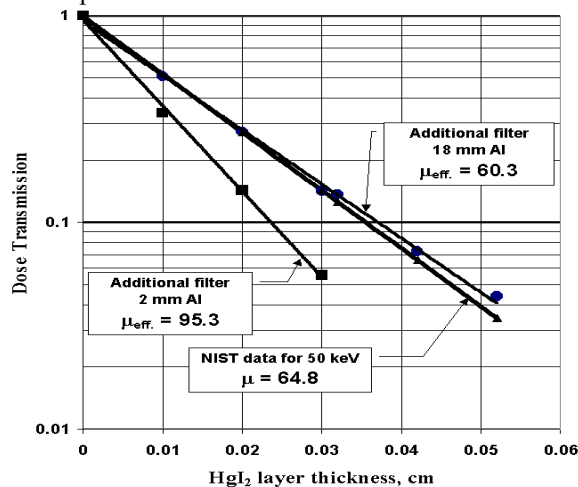


Fig 3. X-Ray dose transmission vs.  $HgI_2$  thickness

### 3.2 Dark currents

Dark current can limit the use of a material for X-ray detection, since it prevents application of high field to optimize the charge collection. High dark current will be stored in the storage capacitance and will limit the dynamic range of the imager. In addition, it will add to the total noise level of the imager. The typical leakage current of HgI<sub>2</sub> PVD films is shown in Fig 4 for a 4" square detector. This detector consisted of an ITO coated substrate upon which HgI<sub>2</sub> was deposited by the PVD process. Top electrodes were then deposited onto the mercuric iodide top surface in a distributed pattern across the substrate. The film leakage current was found to be ~10 pA/mm<sup>2</sup> at 0.5 V/μm, which is significantly reduced compared to earlier published results<sup>2</sup>. There is, however, a degree of variation in the dark current. The dark current standard deviation between electrodes is about 20% of the average value for all fields of 0.3 V/μm and higher.

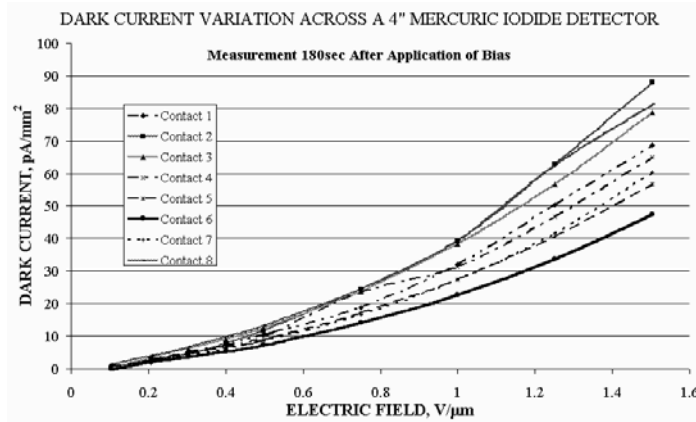


Fig 4. Dark Current vs. bias uniformity across 4"x4" substrate

The temperature dependence of the dark current was also evaluated. This measurement was carried out in a thermostatically controlled, lightproof testing box, enabling precise temperature monitoring and uniformity of testing conditions. The testing rig used consisted of a laboratory oven having 0.1°C temperature resolution, a Keithley picoammeter and a power supply with computer controlled biasing. The temperature dependence of the dark current is shown in Figure 5. From the slope of the curve, it is possible to calculate the activation energy for the leakage current for HgI<sub>2</sub>. Fig 5 shows an activation energy of 1.055 eV.

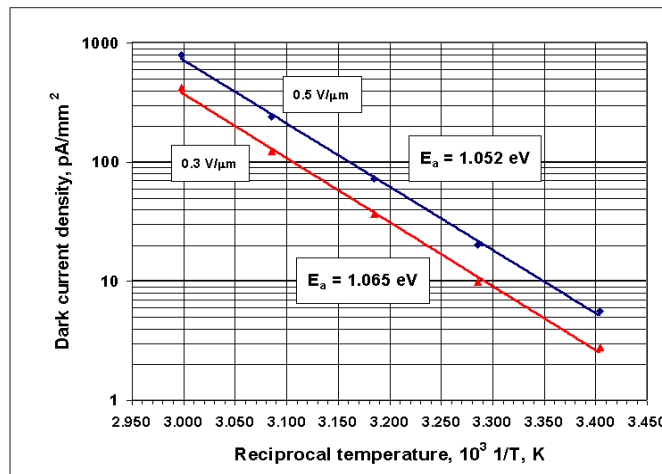


Fig. 5. Dark current vs. temperature measured on PVD detector at 0.3V/μ and 0.5V/μ

### 3.3 Signal

The same 4" square detector that was used to characterize dark current uniformity was also used to evaluate uniformity of X-ray signal response of the PVD mercuric iodide film. The detector was exposed to 380 mR/min of 80kVp X-ray radiation for 4.6 minutes and the signal response was recorded for all electrodes distributed across the substrate. The signal uniformity is significantly better than observed for the detector's dark current. For voltage bias of 0.5 V/ $\mu\text{m}$  and above, the standard deviation of signal response is about 6.7% of the average response across all electrodes. Figure 6 presents the signal response for the detector electrodes in terms of the X-ray sensitivity, measured in units of  $\mu\text{C}/\text{R}\cdot\text{cm}^2$ .

Although non-uniformity of dark current is moderately high, its average value is quite low and it will therefore add little to signal noise. This means that it is the uniformity of X-ray sensitivity across the mercuric iodide photoconductor that will determine the ultimate resolution and gray scale that can be achieved in a full TFT array imager. Although further improvement is desirable, the present result of signal uniformity allows the achievement of high quality X-ray imaging.

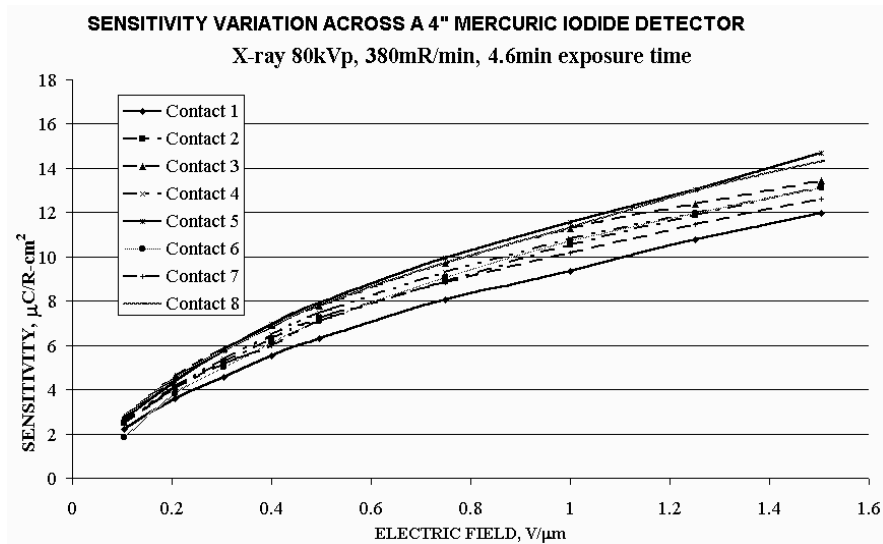


Fig 6. Signal response (sensitivity) as a function of bias voltage for electrodes distributed across a 4"×4" detector

## 4. PIXEL TO PIXEL UNIFORMITY

### 4.1 TFT array image sensor and measuring system

The measurements were performed on 512 x 512 pixel arrays having a pixel size of 100  $\mu\text{m}$  x 100  $\mu\text{m}$ . However, the fabrication processes used are inherently scalable to the large areas required for medical imaging. The pixel design is typical for direct detection devices, and has been described elsewhere<sup>10</sup>. The source contact of the amorphous silicon TFT is connected to the contact electrode, which is isolated from the rest of the pixel by an insulation layer, and the TFT gate and drain are connected to address lines for readout. The contacts are almost square, with a minimum separation to the neighboring pads of 15 $\mu\text{m}$ , and has a geometrical fill factor of 67%.

## 4.2 Signal

Measurement of the electron charge collection is shown in Figure 7. From the figure, one can extract the  $\mu\tau$  of the detector which gives essentially the same  $\mu\tau$  value of  $\sim 1.5 \times 10^{-5} \text{ cm}^2/\text{V}$  for the two measurements<sup>10</sup>.

The initial distribution of carriers depends on the X-ray energy. For low energies (i.e. 24 kVp), the absorption is essentially in a region close to the top contact and in this case, there is a high degree of certainty that the carriers being collected are electrons, and that holes contribute little to the signal. For high energy exposure, the absorption is more uniform throughout the sample, and there may be contributions from both types of carriers.

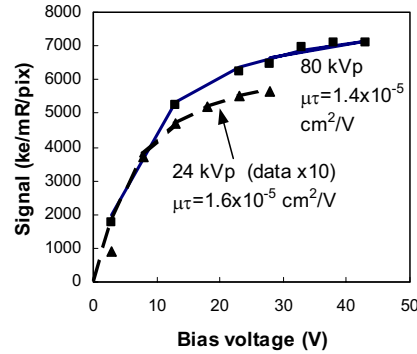


Figure 7. Electron charge collection for  $\text{HgI}_2$  measured at 24 and 80 kVp exposure

## 4.3 Pixel to pixel uniformity

Figure 8 shows pixel-to-pixel uniformity at various exposures for 80 kVp. The dark current background has been subtracted so that broadening of the histogram peaks is due to photon noise and non-uniformity of the pixel response. The sample was exposed by a x-ray beam of 80kVp and average energy per photon ( $E_{\text{avg}}$ ) of 52.3 keV. One can see that the “net” pixel-to-pixel fluctuations obtained decreases with increasing dose. This can be explained by the dependence of gain variance on the dose, namely the dependence of absorption process, charge creation by hot photo-electrons, and charge collection (including traps filling) on dose. This result is a significant improvement relative to that formerly reported<sup>8</sup>.

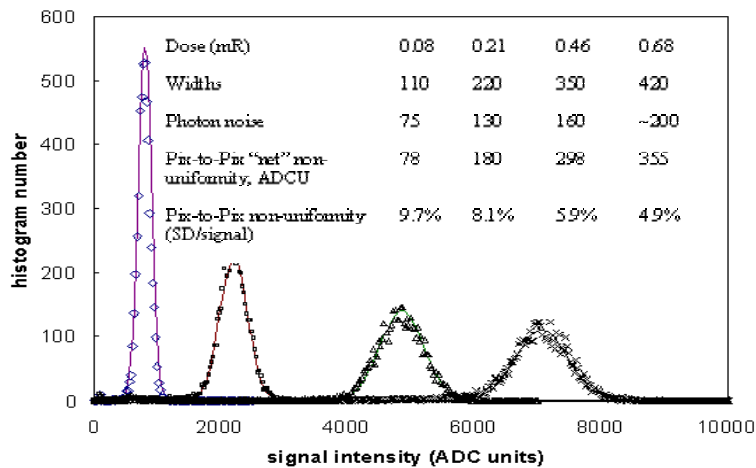


Figure 8. Pixel-to-pixel uniformity is shown at various exposures for 80KVp. The improvement in the micro-uniformity relatively to former results<sup>8</sup> is significant.

## 5. IMAGING WITH TFT ARRAYS

Figure 9 exhibits lag for a mercuric iodide PVD imager when biased at 200V. A continuous 60kVp X-ray beam was applied and then switched off, then charge was collected at the rate of 15 frames/sec. From this graph, charge collection in the first image frame after X-ray illumination is seen to be ~80% of the total generated charge (charge collection is arbitrarily defined as 100% in the first frame while 22.6% additional cumulative charge is collected in the following 14 frames).

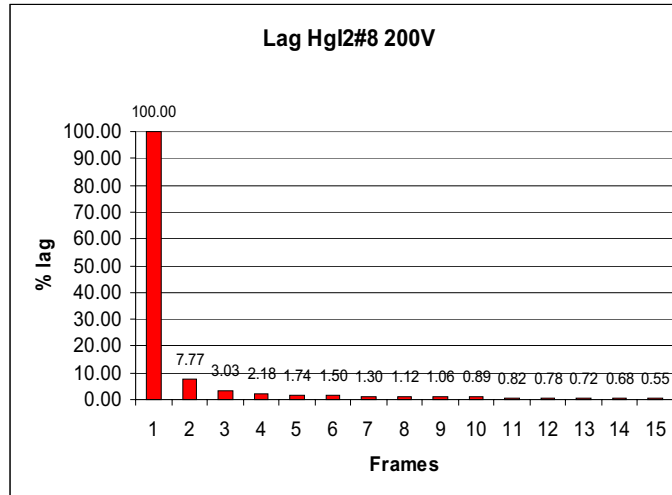


Fig 9 . Lag measured for a PVD mecuric iodide at 15 frames per second.

The excellent resolution was confirmed by imaging a resolution test phantom shown in Figure 10. The measurements and the image were taken in continuous fluoroscopic mode at 60-kVp X-ray energy and 2.1mA current. The imager runs at 15 frame/sec. The dose rate was 0.29mR/frame. The lines are well distinguishable up to the 3.9 lp/mm range (see insert) so the resolution was essentially limited only by the pixel size.

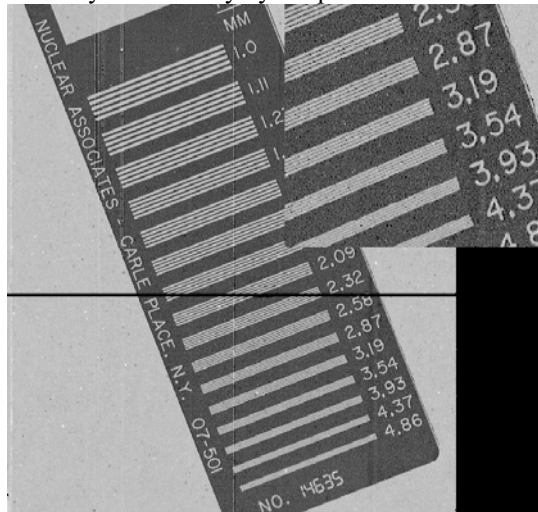


Fig.10. Resolution pattern image obtained with a pixilated amorphous silicon substrate coated with a 165  $\mu\text{m}$  HgI<sub>2</sub> film deposited by PVD on a 127 $\mu\text{m}$  pixel size TFT array. Excellent resolution is achieved

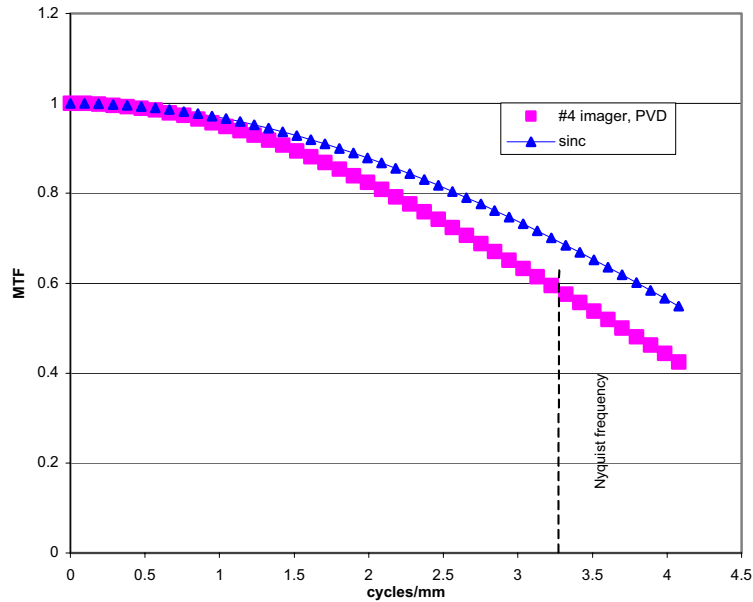


Fig. 11. MTF of a PVD deposited  $\text{HgI}_2$  imager with  $139\mu\text{m}$  pixel size. The theoretical sinc function is also plotted for reference

As a more qualitative gauge of the resolution, we also measured the Modulation Transfer Function (MTF) of an imager with  $139\mu\text{m}$  pixel pitch (Fig. 11). For these tests,  $60\text{kVp}$  x-ray energy and  $290\mu\text{R}$  dose/frame were used. The MTF is only slightly below the theoretical sinc function up to the Nyquist frequency ( $\sim 3.6\text{lp/mm}$ ) given by the  $139\mu\text{m}$  pixel size. This shows that the resolution is practically limited only by the pixel size. By decreasing the pixel size, we can get higher resolutions using  $\text{HgI}_2$  material.

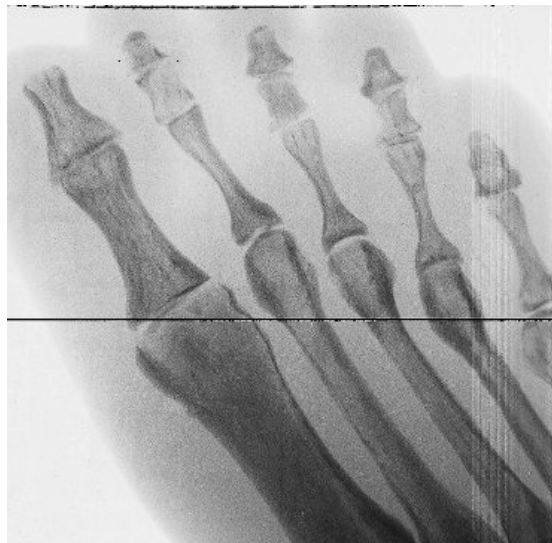


Fig. 12. Foot phantom image taken by a  $4'' \times 4''$  size imager.

Finally, we took a foot phantom image by an  $\text{HgI}_2$  imager with  $127\mu\text{m}$  pixel size (Fig 12). The fine structures of the bones are clearly visible. This image demonstrates that the image quality of the  $\text{HgI}_2$  imagers (even on larger sizes) are getting better and approaching that of the medical requirements.

## 6. SUMMARY

Images obtained with 4"x4" and 2"x2" imaging pixilated arrays using PVD-HgI<sub>2</sub> films are shown. The HgI<sub>2</sub> arrays demonstrate high sensitivity to x-rays and excellent spatial resolution. Extremely high resolution and high absorption were also shown. This suggests new applications for HgI<sub>2</sub> detectors, especially those requiring extreme sensitivity such as fluoroscopy, which is beyond the capabilities of thin film detectors.

## 7. ACKNOWLEDGMENTS

The authors are grateful to the members of the RTR Testing group, I. Baydjanov and M. Kaminsky for carrying out the tests of X-Ray absorption and dark current dependence on temperature.

## 8. REFERENCES

1. **"Mercuric Iodide Thick Films for Radiological X-ray Detectors"**. M. Schieber, H. Hermon, R.A. Street, S.E. Ready, A. Zuck, A. Vilensky, L. Melekhov, R. Shatunovsky, M. Lukach, E. Meerson, Y. Saado and E. Pinhasy, Proc. of the SPIE Vol. 4142 (2000) 197.
2. **"Radiological X-ray Response of Polycrystalline Mercuric Iodide Detectors"**. M. Schieber, H. Hermon, R. Street, S. Ready, A. Zuck, A. Vilensky, L. Melekhov, R. Shatunovsky, E. Meerson, Y. Saado. In Proc. of the SPIE on Medical Imaging 2000 San Diego, Vol. 3977 (2000) 48.
3. **"Theoretical and experimental sensitivity to X-rays of single and polycrystalline HgI<sub>2</sub> compared with different single crystal detectors"**. M. Schieber, H. Hermon, A. Zuck, A. Vilensky, L. Melekhov, R. Shatunovsky, E. Meerson, H. Saado, NIMA Vol. 458 (2001) p 41.
4. **"Characterization of CZT Detectors Grown From Horizontal and Vertical Bridgman"**. H. Hermon, M. Schieber, M. Goorsky, T. Lam, E. Meerson, H. Yao, J. Erickson, and R.B. James, in Proc. of the SPIE on Hard X-ray and Gamma-ray Radiation, Vol. 4141 (2000) 186.
5. **"Comparison of Cadmium Zinc Telluride Crystals Grown by Horizontal and Vertical Bridgman and From the Vapor Phase"**. M. Schieber, R.B. James, H. Hermon, A. Vilensky, I. Baydjanov, M. Goorsky, T. Lam, E. Meerson, H.W. Yao, J. Erickson, E. Cross, A. Burger, J.O. Ndap, G. Wright, and M. Fiederle, Accepted for publication in JCG (2001).
6. **"Thick Films of X-Ray Polycrystalline Mercuric Iodide Detectors"**. M. Schieber, H. Hermon, A. Zuck, A. Vilensky, L. Melekhov, R. Shatunovsky, E. Meerson, Y. Saado, M. Lukach, E. Pinhasy, S.E. Ready, and R.A. Street, Journal of Crystal Growth, 225 (2-4) (2001) pp. 118-123.
7. **"Deposition of Thick Films of Polycrystalline Mercuric Iodide X-Ray Detectors"**. H. Hermon, M. Schieber, A. Zuck, A. Vilensky, L. Melekhov, E. Shtekel, A. Green, O. Dagan, S.E. Ready, R.A. Street, G. Zentai, and L. Partain, Proc. of the SPIE, MI 2001 – Vol. 4320 (2001) pp. 133-139.
8. **"Comparative Study of PbI<sub>2</sub> and HgI<sub>2</sub> as Direct Detector Materials for High Resolution X-ray Image Sensors"**. R.A. Street, M. Mulato, S.E. Ready, R. Lau, J. Ho, K. VanSchuylenbergh, M. Schieber, H. Hermon, A. Zuck, A. Vilensky, K. Shah, P. Bennett and Y. Dmitryev. Proc. of the SPIE MI 2001 - Vol. 4320 (2001) pp. 1-12.

9. **“Non Destructive Imaging with Mercuric Iodide Thick Film X ray detectors”**. M. Schieber, H. Hermon, A. Zuck, A. Vilensky, L. Melekhov, M. Lukach, E. Meerson, Y. Saado, E. Shtekel, B. Reisman, G. Zentai, E. Seppi, R. Pavlyuchkova, G. Virshup, L. Partain, R. Street, S.E. Ready and R. James. Published in Proc. of the SPIE NDT 2001 - Vol. 4335 (2001) pp. 43-51.
  
10. **“Comparison of PbI<sub>2</sub> and HgI<sub>2</sub> for Direct Detection Active N=Matrix X –Ray Image Sensor”** R.A. Street, S.E. Ready, K.V. Schuylenbergh, J. Ho, J.B. Boyce, P. Nylen, K. Shah, L. Melekhov and H. Hermon J. App. Phys. Vol 91, No 5 P 3345 (2002).
  
11. **“Approaching the Theoretical X-ray Sensitivity with HgI<sub>2</sub> Direct Detection Image Sensors”**. R.A. Street, S.E. Ready, L. Melekhov, J. Ho, A. Zuck and B. Breen. To be published in Proc. of the SPIE MI 2002.
  
12. **“Large Area Mercuric Iodide X-Ray Imager”**. G. Zentai, L. Partain, R. Pavlyuchkova, G. Virshup, A. Zuck, L. Melekhov, O. Dagan, A. Vilensky and H. Gilboa. To be published in Proc. of the SPIE MI 2002.
  
13. **“Large area mercuric iodide thick film X-ray detectors for fluoroscopic (on-line) imaging”**. G. Zentai, L. Partain, R. Pavlyuchkova, C. Proano, G. Virshup, B.N. Breen, A. Zuck, B. Reisman, A. Taieb and M. Schieber. To be published in Proc. of the SPIE NDT 2002.
  
14. **“Technology and Applications of Amorphous Silicon”** R. A. Street, ed., Springer, 1999. JM Boone, JA Seibert, Med. Phys. 24 (1997), 1661-1670.
  
15. <http://physics.nist.gov/PhysRefData/XrayMassCoef/cover.html>, JH Hubbell, SM Seltzer, (NIST public domain).
  
16. **“Handbook of Medical Imaging” Vol 1**, JM Boone in (J Beutel, HL Kundel, RL Van Metter, eds.), SPIE Press 2000.
  
17. **“X-Ray Imaging Using Amorphous Selenium: Feasibility of a Flat Panel Self- Scanned Detector for Digital Radiology”** W Zhao, JA Rowlands, Med. Phys. 22 (1995), 1595-1604.